

Three-dimensional stability of leapfrogging quantum vortex rings

Victor P. Ruban*

L.D. Landau Institute for Theoretical Physics RAS, 142432 Chernogolovka, Moscow region, Russia

(Dated: August 27, 2018)

It is shown by numerical simulations within a regularized Biot-Savart law that dynamical systems of two or three leapfrogging coaxial quantum vortex rings having a core width ξ and initially placed near a torus of radii R_0 and r_0 , can be three-dimensionally (quasi-)stable in some regions of parameters $\Lambda = \ln(R_0/\xi)$ and $W = r_0/R_0$. At fixed Λ , stable bands on W are intervals between non-overlapping main parametric resonances for different (integer) azimuthal wave numbers m . The stable intervals are most wide ($\Delta W \sim 0.01-0.05$) between m -pairs (1, 2) and (2, 3) at $\Lambda \approx 4-12$ thus corresponding to micro/mesoscopic sizes of vortex rings in the case of superfluid ^4He . With four and more rings, at least for $W > 0.1$, resonances overlap for all Λ and no stable domains exist.

PACS numbers: 47.32.C-, 47.37.+q, 67.25.dk

I. INTRODUCTION

Dynamics of coaxial vortex rings in a fluid was considered by many authors starting from Helmholtz (see, e. g., [1–4], and numerous references therein). In ordinary fluid, a finite-core vortex ring is subjected to short-scale instabilities which deform cross section of the core and prevent the ring from a distant propagation (see [5–9], and references therein). In contrast, quantized vortices in superfluid ^4He at low temperature (helium-II) behave much like purely one-dimensional objects and are known to be intrinsically stable (because quantum vortex rings and filaments in ^4He do exist and are observed experimentally for macroscopic times [10–13]). Therefore, instabilities can occur only when $N \geq 2$ quantum rings interact. In this context, a particularly interesting dynamical regime is the so called leapfrogging motion of two or more coaxial vortex rings when they periodically pass through one another infinitely many times, as exemplified in Fig.1 (for a review, see [3, 4]). While investigated in detail for idealized axially symmetric configurations, interacting quantum vortex rings with distortions in three dimensions were theoretically considered just in a few recent works [14–18]. In particular, perturbations of vortex ring pairs were studied analytically in [17, 18], but with parameters corresponding to short-scale instabilities. Numerical simulations of macroscopic-size toroidal vortex bundles in Ref. [15] demonstrated development of three-dimensional (3D) instabilities. In the last case the ratio of central torus radius R_0 to a vortex core width ξ was of order $R_0/\xi \sim 10^8$, thus corresponding to value of the local induction parameter $\Lambda = \ln(R_0/\xi) \approx 18$.

In the present work, it will be demonstrated numerically that systems of two or three leapfrogging coaxial quantum vortex rings with not so large $\Lambda = 4-12$ can be 3D-stable and propagate almost unchanged over many hundreds of initial diameters. Whether the motion is stable at given Λ , it strongly depends on another param-

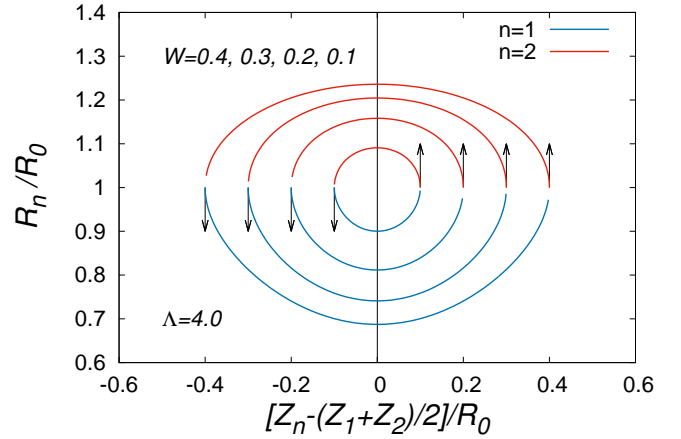


Figure 1: Unperturbed leapfrogging of two coaxial vortex rings in the moving frame of reference. Trajectories of vortices in an axial plane are closed, and they form cross sections of deformed tori. Both vortices move along the same trajectory, but shifted in time on a half-period. At given W , the trajectory passes points $z/R_0 = \pm W$, $r/R_0 = 1$.

eter, $W = r_0/R_0$, where r_0 is a poloidal (smaller) torus radius describing initial vortex configuration. A general explanation of the stability origin is the following. Let shapes of perturbed vortex rings be given in polar coordinates as N pairs of functions

$$Z_n(\varphi, t) = Z_n^{(0)}(t) + \text{Re} \sum_{m \geq 1} z_n^{(m)}(t) \exp(im\varphi), \quad (1)$$

$$S_n(\varphi, t) = S_n^{(0)}(t) + \text{Re} \sum_{m \geq 1} s_n^{(m)}(t) \exp(im\varphi), \quad (2)$$

where $n = 1, \dots, N$, and $S_n(\varphi, t) = R_n^2(\varphi, t)/2$ is canonically conjugate to $Z_n(\varphi, t)$. The crucial point is that 3D instabilities are parametric in their nature, because linearised equations of motion for $z_n^{(m)}(t)$ and $s_n^{(m)}(t)$ contain (real) time-dependent coefficients depending on

*Electronic address: ruban@itp.ac.ru

$Z_n^{(0)}(t)$ and $S_n^{(0)}(t)$,

$$\dot{z}_n^{(m)} = \sum_{n'} [A_{n,n'}^{(m)}(t)s_{n'}^{(m)} + B_{n,n'}^{(m)}(t)z_{n'}^{(m)}], \quad (3)$$

$$-\dot{s}_n^{(m)} = \sum_{n'} [B_{n',n}^{(m)}(t)s_{n'}^{(m)} + C_{n,n'}^{(m)}(t)z_{n'}^{(m)}], \quad (4)$$

where matrices $A^{(m)}$ and $C^{(m)}$ are symmetric, with dominating (at $m \geq 2$, $\Lambda \gg 1$) diagonals, while $B^{(m)}$ has zeroes everywhere on the diagonal. Consider for the moment a purely periodic unperturbed leapfrogging with a time period T . Then all the coefficients in Eqs.(3)-(4) are time-periodic with this period. It is always the case for $N = 2$, but for $N = 3$ there also exist periodic solutions (so called relative choreographies [4]). We will imply that the rings are on a (stationary moving) deformed torus having a z -size $2r_0$ and a mean r -size R_0 from z -axis (see Fig.1). Previous simulations have shown that period T of relative axisymmetric motion depends on Λ and W [3, 4]. According to general mathematical theory, characteristic multipliers of our linear Hamiltonian system (3)-(4) with time-periodic coefficients have the form

$$\rho_{\pm,i}^{(m)} = \exp\left(\pm \sqrt{\mu_i^{(m)}} T\right), \quad i = 1, \dots, N, \quad (5)$$

where $\mu_i^{(m)}(\Lambda, W)$ are real functions. If at least one of them is positive, then the motion is parametrically unstable at given Λ and W . Qualitatively, this phenomenon is similar to well-known parametric instabilities for a single oscillator described by equation $\eta_{\tau\tau} + [\alpha + \delta \cos(\tau)]\eta = 0$ with parameters α and δ (parametric resonances take place near $\alpha = (p/2)^2$, with $p = 1, 2, \dots$, while the corresponding increments $\gamma_p \sim \delta^p$). Let us in our case introduce a discrete index \tilde{p} which enumerates positive ‘‘humps’’ of $\mu_{\max}^{(m)}(\Lambda, W)$ at a fixed Λ . Among them there are the most ‘‘dangerous’’ (main) parametric resonances. Our simulations for $N = 2$ and $N = 3$ (in the last case the unperturbed relative motion was actually only approximately periodic) have shown that at relatively small $\Lambda \lesssim 3$, neighboring main parametric resonances overlap on parameter W . With larger $\Lambda = 4-8$ however, intervals between resonances appear at $W \approx 0.2-0.25$ and reach widths of order $\Delta W \sim 0.01-0.05$ (the intervals are more prominent for $N = 2$). At even larger $\Lambda \gtrsim 15$ (macroscopic sizes of rings), stable intervals are shifted towards smaller $W \lesssim 0.15$ (thin tori).

Strictly speaking, secondary parametric resonances also contribute to overall instability, especially for $N = 3$, but they are weaker and not so wide to close stable ‘‘windows’’ completely.

The structure of main instabilities in the case of coaxial rings turned out to be relatively simple, in contrast to recently observed numerically but yet unexplained analytically, qualitatively similar instabilities of torus quantum vortex knots and links [19, 20].

II. APPROXIMATE DYNAMICAL MODEL

Apparently, the main characteristics of instabilities are functions $\mu_i^{(m)}(\Lambda, W)$. In general, they could be extracted by a complicated procedure from analysis of linearized equations of motion (3)-(4). However, in this work we actually do not take that way, since matrices $A^{(m)}(t)$, $B^{(m)}(t)$, and $C^{(m)}(t)$ are very cumbersome expressions involving special functions even in the simplest case $N = 2$ [17, 18]. Instead, we employ a different approach and simulate the motion of vortex rings numerically until their significant deformation, thus including nonlinear stages of instabilities into consideration (see three examples in Fig.2). At the end of each run, we obtain an estimate for lifetime of vortex system at given values of initial parameters (and we believe the estimate is close to what could be observed in a real situation). After that we collect data and present the results as plots for inverse lifetime depending on W , for different Λ . Our numerical experiments are based on a simplified but quite accurate mathematical model, discussed below.

To describe dynamics of vortex rings in three dimensions, we treat them in a usual manner as closed smooth space curves determined by N vector functions $\mathbf{X}_n(\beta, t)$ depending on an arbitrary longitudinal parameter β and time t . We adopt a regularized Biot-Savart law in the form (see [19–21] and compare to [22–24])

$$\dot{\mathbf{X}}_n(\beta, t) = \sum_{j=1}^N \frac{\Gamma}{4\pi} \oint \frac{\tilde{\mathbf{X}}_j' \times (\mathbf{X}_n - \tilde{\mathbf{X}}_j)}{\sqrt{(|\mathbf{X}_n - \tilde{\mathbf{X}}_j|^2 + a^2)^3}} d\tilde{\beta} + \frac{\Gamma\lambda}{4\pi} \varkappa_n \mathbf{b}_n, \quad (6)$$

where $\Gamma = 2\pi\hbar/m_{\text{at}}$ is the circulation quantum (with atomic mass m_{at}), $\tilde{\mathbf{X}}_j = \mathbf{X}_j(\tilde{\beta}, t)$, $\tilde{\mathbf{X}}_j' = \partial\mathbf{X}_j(\tilde{\beta}, t)/\partial\tilde{\beta}$, $\varkappa_n(\beta, t)$ is a local curvature of the filament (in the usual geometric sense), and $\mathbf{b}_n(\beta, t)$ is a local unit binormal vector on the curve. Here λ is a (positive) stiffness parameter characterizing potential energy of quantum vortex core, and $a = \xi \exp(\lambda)$ is a geometric core radius. Note that the last term in Eq.(6) corresponds formally to the local induction approximation (LIA), while the sum of nonlocal integrals is a smoothly regularized Biot-Savart law for vorticity distribution in the form of several infinitely thin filaments, each having one quantum of circulation. Thus, we define an effective core width ξ in such a manner that the total local induction parameter is $\Lambda = \lambda + \ln(R_0/a) = \ln(R_0/\xi)$.

The presence of two parameters, a and λ , makes the model quite flexible to quantitatively describe relatively long-scale dynamics of real vortices in a superfluid.

For simplicity, we work with non-dimensionalized quantities, so that formally $\Gamma = 2\pi$, $R_0 = 1$.

The model under consideration is a Hamiltonian system, with non-canonical structure $[\mathbf{X}'_n \times \tilde{\mathbf{X}}_n] = \delta\mathcal{H}/\delta\mathbf{X}_n$,

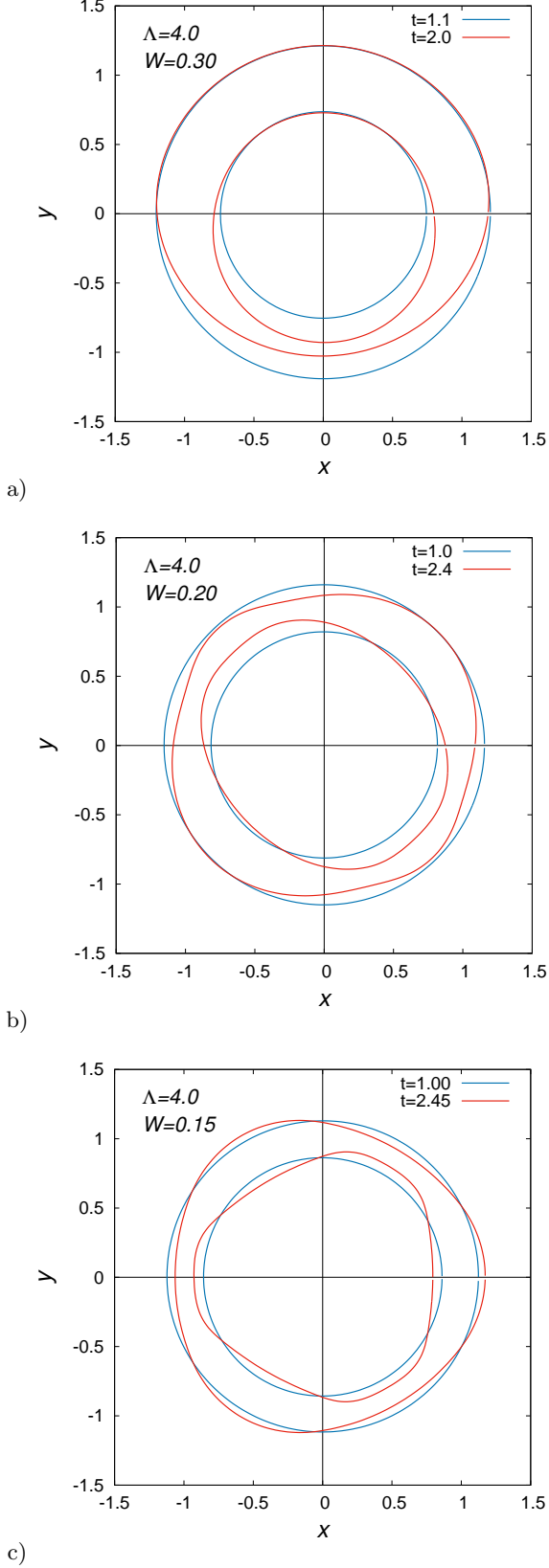


Figure 2: Examples of instability development in a system of two vortex rings for: a) $m = 1$; b) $m = 2$; c) $m = 3$.

and the Hamiltonian functional

$$\mathcal{H} = \frac{1}{4} \sum_{n,j} \oint \oint \frac{(\mathbf{X}'_n \cdot \tilde{\mathbf{X}}'_j) d\beta d\tilde{\beta}}{\sqrt{|\mathbf{X}_n - \tilde{\mathbf{X}}_j|^2 + a^2}} + \frac{\lambda}{2} \sum_n \oint |\mathbf{X}'_n| d\beta. \quad (7)$$

In this expression, the double sum of non-local terms corresponds to kinetic energy of superfluid flow created by quantized vortices, while the ordinary sum of local integrals is potential energy of the cores.

Canonically conjugate functions are different in different curvilinear coordinate systems. For example, when parameterized by the azimuthal angle in polar coordinates, $Z_n(\varphi, t)$ and $R_n^2(\varphi, t)/2$ are canonical variables. Matrices $A^{(m)}$, $B^{(m)}$, and $C^{(m)}$ as functions of $Z_n^{(0)}$ and $S_n^{(0)}$ then follow from expansion of the correspondingly expressed Hamiltonian in azimuthal perturbations up to the second order. We do not write them here.

Although physical applicability of the above hydrodynamical model is restricted to relatively long scales $\tilde{l} \gg a$, but in numerical simulations short scales of order a can be also important.

It is parameter λ that prevents short-scale instabilities (compare with [25] where it was not included). Indeed, let us consider a straight vortex filament. Small perturbations $X(z, t)$ and $Y(z, t)$ are canonically conjugate in that case and described by quadratic Hamiltonian

$$\begin{aligned} \mathcal{H}^{(2)} &= \frac{1}{4} \iint \frac{(X' \tilde{X}' + Y' \tilde{Y}') dz d\tilde{z}}{\sqrt{(z - \tilde{z})^2 + a^2}} \\ &\quad - \frac{1}{8} \iint \frac{[(X - \tilde{X})^2 + (Y - \tilde{Y})^2] dz d\tilde{z}}{\sqrt{[(z - \tilde{z})^2 + a^2]^3}} \\ &\quad + \frac{\lambda}{4} \int (X'^2 + Y'^2) dz. \end{aligned} \quad (8)$$

The corresponding dispersion law is

$$\begin{aligned} \omega_q &= \frac{q^2}{2} \left[\lambda + 2K_0(qa) - \frac{2}{(qa)^2} + \frac{2K_1(qa)}{qa} \right] \\ &= \frac{q^2}{2} [\lambda + \tilde{F}(qa)], \end{aligned} \quad (9)$$

with K_0 and K_1 being the modified Bessel functions. It should be noted that different core models result in different expressions for ω_q (see, e.g., [26–28], and references therein). However, with appropriate choice for λ , the present model is able to approximate them very closely. In particular, Lord Kelvin's [26] dispersion relation for ν -th azimuthal mode of a hollow-core columnar vortex can be represented as follows:

$$\omega_{\nu,q}^{L.K.} = \frac{1}{a^2} \left[\pm \left(\nu + qa \frac{K_{\nu-1}(qa)}{K_{\nu}(qa)} \right)^{1/2} - \nu \right], \quad (10)$$

with $\nu = 0, 1, \dots$. We are interested in the soft bending mode which corresponds to $\nu = 1$ and sign “+”. The value $\lambda = 0.5$ works in this case very well (see Fig.3).

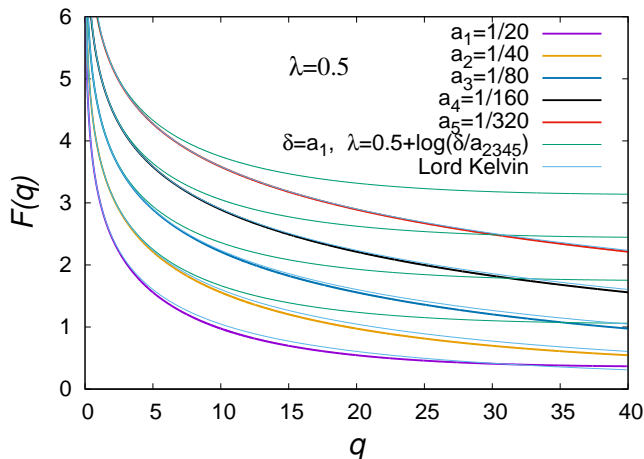


Figure 3: Comparison between “exact” and approximate dispersion laws for a straight vortex filament having a stiffness parameter $\lambda = 0.5$. Plots for $F(q) = 2\omega_q/q^2$ are shown. Also curves corresponding to Lord Kelvin’s dispersion relation (10) for $\nu = 1$ and sign “+” are drawn. The two expressions (9) and (10) are remarkably close to each other.

A more complicated dispersion equation for a constant-vorticity core [26] is not discussed here.

It is important that at small $u \ll 1$, function $\tilde{F}(u) \approx \ln(1/u) > 0$, while at $u_0 \approx 1.1$ it changes the sign, and at $u_* \approx 2.32$ it has a minimum where $\tilde{F}_{min} \approx -0.137$. Therefore, with zero or small λ , frequency $\omega_q = q^2[\lambda + \tilde{F}(qa)]/2$ is small somewhere at $qa \sim 1$. When in a weak externally imposed transverse strain field [so that $\Delta\mathcal{H}^{(2)} = (\sigma/2) \int (X^2 - Y^2) dz$], rectilinear vortex modifies its dispersion law,

$$\Omega_q = \sqrt{\omega_q^2 - \sigma^2}, \quad (11)$$

and instability can occur if the expression under square root becomes negative (concerning a vortex filament in ordinary fluid under external strain, see [29–32]). In context of present work, a local strain on a ring is inevitably caused by its circular shape and by nonuniform velocity field from other rings. Thus, a sufficiently large value of $\lambda > 0.137$ is required to remove such instability.

We do not know a best fit for λ , say, in real superfluid ^4He , but fortunately, it is not so important for our purposes. Indeed we need to simulate just relatively long-scale dynamics corresponding to $q \lesssim 10$ (because $q \sim m$, and we are interested in moderate m). In that domain, the dynamics depends mostly on the total local induction parameter Λ , and does not “feel” actual value of a . Therefore one can replace parameters in the equations of motion (6) without significant loss of accuracy:

$$a \rightarrow \delta, \quad \lambda \rightarrow \lambda + \ln(\delta/a), \quad (12)$$

where $\delta > a$ (of course, vortex configuration should be far from mutual and self-intersections). Fig.3 indicates

that replacement (12) only weakly changes dispersion law at moderate wave numbers. A direct way to see weak sensitivity of the system under (12) is to write in Eq.(7):

$$\frac{1}{\sqrt{|\Delta\mathbf{X}|^2 + a^2}} = \frac{1}{\sqrt{|\Delta\mathbf{X}|^2 + \delta^2}} + \left[\frac{1}{\sqrt{|\Delta\mathbf{X}|^2 + a^2}} - \frac{1}{\sqrt{|\Delta\mathbf{X}|^2 + \delta^2}} \right]. \quad (13)$$

Since the expression in square bracket is effectively local, it approximately results in $(1/2) \ln(\delta/a) \sum_n \delta |\mathbf{X}'_n| d\beta$, thus confirming (12). In most simulations we used $\delta = 1/20$, and only for verification we used $\delta = 1/40$ in some cases. Thus, the major parameters of the system are Λ and W , while a plays a secondary role.

By the way, it is now clear why our model with $\lambda = 1/2$ approximates the Lord Kelvin’s formula for a hollow vortex in ordinary fluid. Indeed, since the core cross section tends to be uniform along the vortex at every time moment, while the volume of core cavity is conserved, we have relation $b^2(t)\mathcal{L}(t) = a^2\mathcal{L}_0$ between actual time-dependent core width $b(t)$ and vortex length $\mathcal{L}(t) = \int |\mathbf{X}'| d\beta$, with constants a and \mathcal{L}_0 . Therefore the Hamiltonian of a single narrow hollow vortex is

$$\mathcal{H}_b \approx \mathcal{H}_a + \frac{1}{2} \ln\left(\frac{a}{b}\right) \mathcal{L} = \mathcal{H}_a + \frac{1}{4} \ln\left(\frac{\mathcal{L}}{\mathcal{L}_0}\right) \mathcal{L}, \quad (14)$$

where \mathcal{H}_a is the a -regularized Biot-Savart Hamiltonian (the first term in Eq.(7)). Quadratic on X and Y part of the above expression is exactly Eq.(8) with $\lambda = 1/2$.

III. NUMERICAL RESULTS

In numerical simulations, terms proportional to \mathbf{X}'_n were added to equations of motion (6), such that azimuthal component of $\tilde{\mathbf{X}}_n$ was equal to zero. Such modification is allowed due to the freedom in choice of the longitudinal parameter β , and it controlled density of distribution of discrete points along the curve.

The same procedure was used as described in Refs.[19, 20]. Basically, it was a pseudo-spectral scheme on the longitudinal parameter β , in combination with a Runge-Kutta 4-th order scheme for time stepping. Shape of each vortex filament was approximated by L points $\mathbf{X}_{n,l}(t) = \mathbf{X}_n(2\pi l/L, t)$ [typical values $L = 256$ and $L = 512$]. At that,

$$\mathbf{X}_{n,l} = \text{Re} \sum_{k=0}^{K-1} \hat{\mathbf{X}}_{n,k} \exp(2\pi ikl/L). \quad (15)$$

In each time step, $K \approx (3/8)L$ of the corresponding Fourier coefficients $\hat{\mathbf{X}}_{n,k}$ participated in the Runge-Kutta procedure. After that, only coefficients with k not higher than $K_{\text{eff}} \approx L/4$ were retained, while the remaining were set to zero. Such strategy has successfully proven itself in many different problems. In our case it also has shown good accuracy and stability.

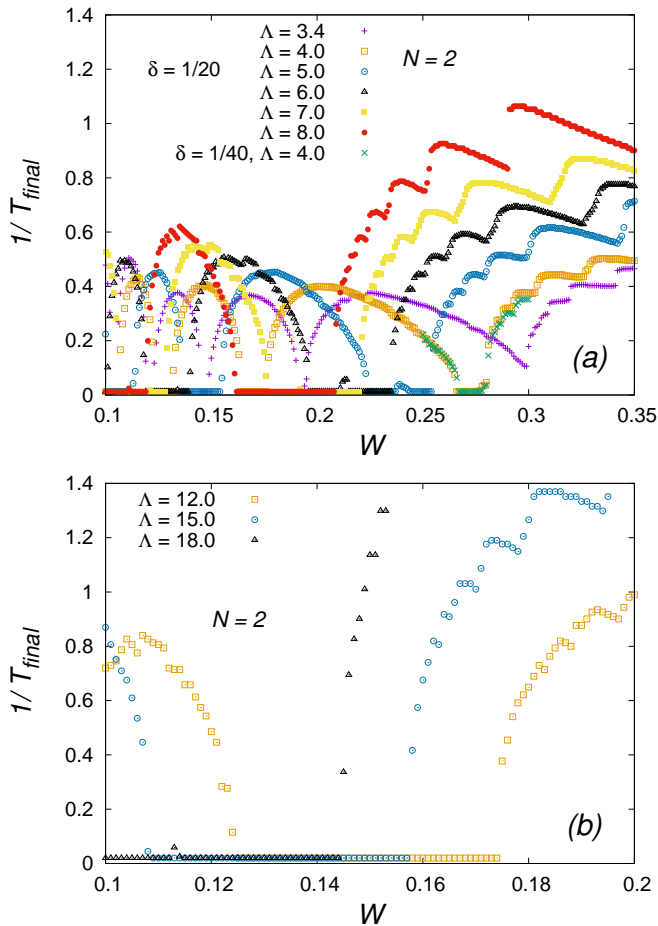


Figure 4: Inverse lifetime for $N = 2$ vortex rings: a) micro/mesoscopic sizes; b) almost macroscopic sizes (here $T_{\text{max}} = 50$). Relatively wide stable bands are seen. For a fixed Λ , the rightest big hump on the plot corresponds to main instability with $m = 1$, the next one to the left is for $m = 2$, and so on. Secondary instabilities are very weak.

For every run, an initial state consisted of N slightly perturbed, nearly coaxial vortex rings placed on a torus with equal poloidal angles between them. More precisely, for $N = 2$ it was a pair of equal rings with unit radius and a distance $2W$ between them. For $N = 3$, it was $Z_n^{(0)}(0) = W \sin(2\pi n/3)$, $R_n^{(0)}(0) = 1 + W \cos(2\pi n/3)$ (of course, these values were not exactly corresponding to a choreography, but the resulting relative motion was nearly periodic, with small superimposed additional oscillations). Typical amplitudes of initial 3D distortions were 0.001–0.01. The run was terminated either when the time reached $T_{\text{max}} = 80$, or when configuration of vortices became close to intersection. A final time T_{final} was recorded, and it was taken as an estimate for vortex system lifetime.

The data collected for $N = 2$ and $N = 3$ are presented in Fig.4 and Fig.5 respectively, which are essentially the main results of present work. Obviously, stable domains,

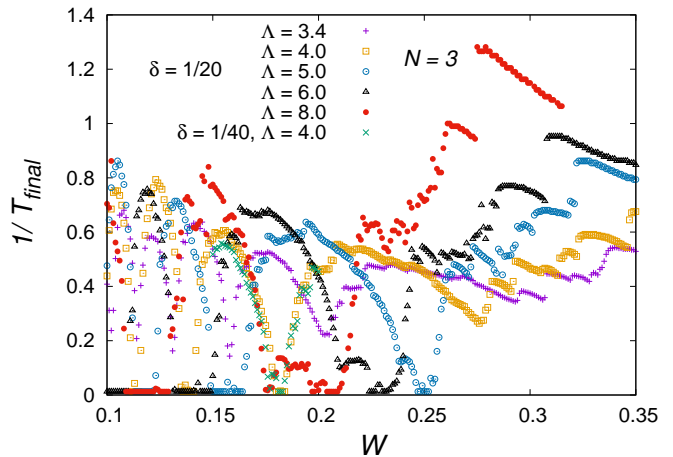


Figure 5: Inverse lifetime for $N = 3$ vortex rings. Here stable bands are not so wide as for $N = 2$, while secondary instabilities are stronger.

if any, should correspond to very small values of the inverse lifetime. Indeed such intervals are clearly seen in the figures. It should be said that Hamiltonian was preserved typically up to 5-6 decimal digits in stable domains. In several additional simulations, T_{max} was equal to 320, and in many cases no tendency to instability development was detected. Leapfrogging vortex rings thus traveled distances as many hundreds of initial diameters.

Especially clean are plots for $N = 2$, because unperturbed relative motion was really periodic. What is interesting, in this case stability of a microscopic-size pair of rings can take place at rather large values $W \approx 0.27$ (Fig.4a), when the corresponding “torus” is “fat” and strongly deformed. The widest stable intervals are between m -pairs (1,2) and (2,3), though they are opened not simultaneously as Λ increases. For almost macroscopic rings with $\Lambda \approx 12$ –18, stable intervals are near $W \approx 0.15$ (Fig.4b).

For $N = 3$, stable bands still exist, though not so wide and spoiled slightly by secondary instabilities. Results for $N = 4$ are not presented because there we did not observe stability zones.

IV. CONCLUSIONS

Thus, accurate numerical simulations based on a widely accepted theoretical model for nonlinear dynamics of quantum vortex rings have been carried out and demonstrated existence of parametrically stable regimes in leapfrogging motion of two and three coaxial rings. The local induction parameter in “optimal” domain $\Lambda \approx 4$ –10 corresponds to micro/mesoscopic sizes of vortex rings, if superfluid ^4He is meant. In that domain, several stable bands were found corresponding to rather appreciable relative distances between the rings (up to

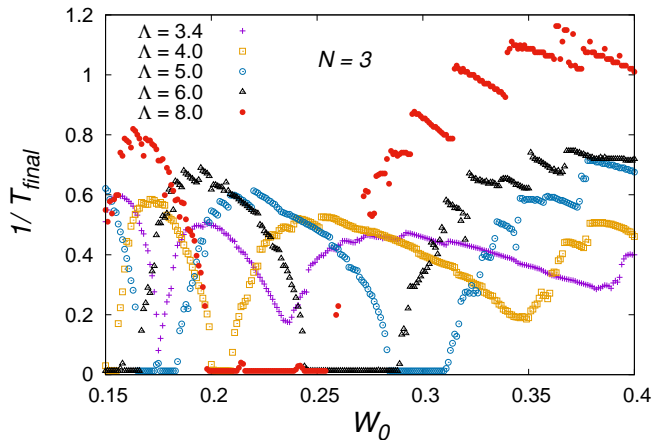


Figure 6: Inverse lifetime for $N = 3$ vortex rings with initial positions closely corresponding to choreographies. Qualitatively, the plots are similar to Fig. 5, but here stable intervals are quite wide.

$2W \approx 0.55$ for the first stable interval).

Further theoretical efforts should perhaps be directed towards immediate calculation of the monodromy matrix for linear system (3)-(4) and finding its eigenvalues $\rho_{\pm, i}^{(m)}$.

A system of three vortex rings can exhibit also a more complicated regime as chaotic leapfrogging [4]. That interesting case has not yet been investigated for 3D stability.

The numerical results obtained here seem interesting and also potentially stimulating for future experiments. Indeed, if one is going to investigate parametrically stable nontrivial vortex configurations in a real-world experiment, then the problem of controllable creation of a few mesoscopic-size coaxial vortex rings can become in practice more easy than creation of vortex knots or links.

After acceptance of the above text for publication in *Physics of Fluids*, additional simulations for three vortex rings were carried out with somewhat different, empirically selected initial ring positions much better corresponding to relative choreographies: $Z_n^{(0)}(0) = W_0 \sin(2\pi n/3)$, $R_n^{(0)}(0) = \sqrt{1 + 2W_0[1 - D(\Lambda)W_0] \cos(2\pi n/3)}$. Here coefficient $D(\Lambda)$ ranges from ≈ 1.0 at $\Lambda = 4.0$ to ≈ 1.16 at $\Lambda = 8.0$. Simulations have shown axial size W of the resulting deformed torus to differ slightly from the auxiliary parameter W_0 , so that $W = W_0 - \mathcal{O}(W_0^2)$. What is important in this case, it is the presence of more wide and clean stability intervals, presented in Fig. 6.

-
- [1] H. Helmholtz, "On integrals of the hydrodynamical equations which express vortex motion," *J. Reine Angew. Math.* **55**, 25 (1858) (in German).
 - [2] K. Shariff and A. Leonard, "Vortex rings," *Annu. Rev. Fluid Mech.* **24**, 235 (1992).
 - [3] V. V. Meleshko, "Coaxial axisymmetric vortex rings: 150 years after Helmholtz," *Theor. Comput. Fluid Dyn.* **24**, 403 (2010).
 - [4] A. V. Borisov, A. A. Kilin, and I. S. Mamaev, "The dynamics of vortex rings: Leapfrogging, choreographies and the stability problem," *Reg. Chaot. Dyn.* **18**, 33 (2013).
 - [5] S. E. Widnall, D. B. Bliss, and C.-Y. Tsai, "The instability of short waves on a vortex ring," *J. Fluid Mech.* **66**, 35 (1974).
 - [6] S. E. Widnall, "The structure and dynamics of vortex filaments," *Annu. Rev. Fluid Mech.* **7**, 141 (1975).
 - [7] S. E. Widnall and C.-Y. Tsai, "The instability of the thin vortex ring of constant vorticity," *Philos. Trans. R. Soc. Lond. A* **287**, 273 (1977).
 - [8] Y. Hattori and Y. Fukumoto, "Short-wavelength stability analysis of thin vortex rings," *Phys. Fluids* **15**, 3151 (2003).
 - [9] Y. Fukumoto and Y. Hattori, "Curvature instability of a vortex ring," *J. Fluid Mech.* **526**, 77 (2005).
 - [10] G. W. Rayfield and F. Reif, "Quantized Vortex Rings in Superfluid Helium," *Phys. Rev.* **136**, A1194 (1964).
 - [11] E. J. Yarmchuk, M. J. V. Gordon, and R. E. Packard, "Observation of Stationary Vortex Arrays in Rotating Superfluid Helium," *Phys. Rev. Lett.* **43**, 214 (1979).
 - [12] G. P. Bewley and K. R. Sreenivasan, "The Decay of a Quantized Vortex Ring and the Influence of Tracer Particles," *J. Low Temp. Phys.* **156**, 84 (2009).
 - [13] P. M. Walmsley, P. A. Tompsett, D. E. Zmeev, and A. I. Golov, "Reconnections of Quantized Vortex Rings in Superfluid ^4He at Very Low Temperatures," *Phys. Rev. Lett.* **113**, 125302 (2014).
 - [14] R. M. Caplan, J. D. Talley, R. Carretero-Gonzalez, and P. G. Kevekidis, "Scattering and leapfrogging of vortex rings in a superfluid," *Phys. Fluids* **26**, 097101 (2014).
 - [15] D. H. Wacks, A. W. Baggaley, and C. F. Barenghi, "Coherent laminar and turbulent motion of toroidal vortex bundles," *Phys. Fluids* **26**, 027102 (2014).
 - [16] T. Zhu, M. L. Evans, R. A. Brown, P. M. Walmsley, and A. I. Golov, "Interactions between unidirectional quantized vortex rings," *Phys. Rev. Fluids* **1**, 044502 (2016).
 - [17] S. S. Gubser, R. Nayar, and S. Parikh, "Strings, vortex rings, and modes of instability," *Nucl. Phys. B* **892**, 156 (2015).
 - [18] S. S. Gubser, B. Horn, and S. Parikh, "Perturbations of vortex ring pairs," *Phys. Rev. D* **93**, 046001 (2016).
 - [19] V. P. Ruban, "Long-Lived Quantum Vortex Knots," *JETP Letters* **107**(5), 307 (2018).
 - [20] V. P. Ruban, "Quasi-stable configurations of torus vortex knots and links," *ZhETF* **154**, 679 (2018) (in Russian); [English translation: *JETP* **127**(3), ??? (2018)].
 - [21] A. Leonard, "Computing 3-dimensional incompressible flows with vortex elements," *Annu. Rev. Fluid Mech.* **17**, 523 (1985).
 - [22] K. W. Schwarz, "Three-dimensional vortex dynamics in superfluid ^4He : Line-line and line-boundary interac-

- tions,” *Phys. Rev. B* **31**, 5782 (1985).
- [23] M. Tsubota, T. Araki, and S. K. Nemirovskii, “Dynamics of vortex tangle without mutual friction in superfluid ^4He ,” *Phys. Rev. B* **62**, 11751 (2000).
- [24] A. W. Baggaley and C. F. Barenghi, “Spectrum of turbulent Kelvin-waves cascade in superfluid helium,” *Phys. Rev. B* **83**, 134509 (2011).
- [25] U. R. Fischer and N. Schopohl, “Short wavelength spectrum and Hamiltonian stability of vortex rings,” *Phys. Rev. E* **64**, 016306 (2001).
- [26] W. Thompson (Lord Kelvin), “Vibrations of a columnar vortex,” *Philos. Mag.* **10**, 155 (1880).
- [27] D. W. Moore and P. G. Saffman, “A note on the stability of a vortex ring of small cross-section,” *Proc. R. Soc. Lond. A* **338**, 535 (1974).
- [28] C. F. Barenghi, R. Hanninen, and M. Tsubota, “Anomalous translational velocity of vortex ring with finite-amplitude Kelvin waves,” *Phys. Rev. E* **74**, 046303 (2006).
- [29] D. W. Moore and P. G. Saffman, “The instability of a straight vortex filament in a strain field,” *Proc. R. Soc. Lond. A* **346**, 413 (1975).
- [30] C.-Y. Tsay and S. E. Widnall, “The stability of short waves on a straight vortex filament in a weak externally imposed strain field,” *J. Fluid Mech.* **73**, 721 (1976).
- [31] A. C. Robinson and P. G. Saffman, “Three-dimensional stability of an elliptical vortex in a straining field,” *J. Fluid Mech.* **142**, 451 (1984).
- [32] Y. Fukumoto, “The three-dimensional instability of a strained vortex tube revisited,” *J. Fluid Mech.* **493**, 287 (2003).